

Meshless Method for Crack Analysis in Functionally Graded Materials with Enriched Radial Base Functions

P.H. Wen¹, M.H. Aliabadi² and Y.W. Liu³

Abstract: Based on the variation of potential energy, the element-free Galerkin method (MFGM) has been investigated for structures with crack on the basis of radial base function interpolation. An enriched radial base function is introduced to capture the singularities of stress at the crack tips. The advantages of the finite element method are remained in this method and there is a significant improvement of accuracy, particularly for the crack problems of fracture mechanics. The applications of the element-free Galerkin method with enriched radial base function to two-dimensional fracture mechanics in functionally graded materials have been presented and comparisons have been made with numerical solutions using different numerical approaches.

Keyword: element-free Galerkin method, functionally graded materials, cracks, enriched radial base function, static and dynamic load, stress intensity factors.

1 Introduction

It is well-known that the finite element method (FEM) is the most widely used numerical method in dealing with linear, nonlinear and large scale problems. However, the finite element method suffers from drawbacks such as the generation of a finite element mesh with thousands of nodes, particularly for the crack propagation and moving boundaries. Although FEM has been very successfully established and applied in engineering as one of the most powerful numerical tools,

the development of new advanced methods nowadays is still attractive in computational mechanics. Meshless approximations have received much interest since Nayroles et al (1992) proposed the diffuse element method. Later, Belyschko et al (1994) and Liu et al (1995) proposed the element-free Galerkin method (EFGM) and reproduced the kernel particle method respectively. One key feature of these methods is that they do not require a structured grid and are therefore meshless. Recently, Atluri and his colleagues presented a family of meshless methods, based on the Local weak Petrov-Galerkin formulation (MLPGs) for arbitrary partial differential equations [see Atluri et al (1998a, 1998b, 1999, 2002, 2004a) with moving least-square (MLS) approximation]. MLPG is reported to provide a rational basis for constructing meshless methods with a greater degree of flexibility. The Meshless Finite Volume Method (MFVM) is developed for solving elasto-static problems, through a new Meshless Local Petrov-Galerkin "Mixed" approach (Atluri 2004b). The general Meshless Local Petrov-Galerkin type weak-forms of the displacement and traction boundary integral equations are derived for solids undergoing small deformations (Atluri 2003). The Meshless Local Petrov-Galerkin mixed collocation method is proposed for solving elasticity problems (Atluri 2006). A comparison study of the efficiency and accuracy of a variety of meshless trial and test functions is studied based on the general concept of the meshless local Petrov-Galerkin method (Atluri 2002). The Finite Difference Method (FDM), within the framework of the Meshless Local Petrov-Galerkin approach, is proposed for solving solid mechanics problems (Atluri 2005). The implementation of a three-dimensional dynamic code, for contact, impact, and penetration mechanics, based on

¹ Department of Engineering, Queen Mary, University of London, London, UK, E1 4NS

² Department of Aeronautics, Imperial College, London, UK, SW7 2BY

³ College of Mechanics and Aerospace, Hunan University, Changsha 410082, PR China

the Meshless Local Petrov-Galerkin approach has been presented (Han 2006). A meshless computational method based on the local Petrov-Galerkin approach for the analysis of shell structures is presented for three dimensional solid, allowing the use of completely 3-D constitutive models (Jarak 2007). A truly meshless method, the Meshless Local Petrov-Galerkin Method, is developed for three-dimensional elasto-statics (Li 2003) and for the problem of topology-optimization of elastic structures (Li 2008). A new scheme, called simplified finite difference interpolation (SFDI), is devised (Ma 2008). A meshless method based on the local Petrov-Galerkin approach is proposed for the solution of boundary value problems for coupled thermo-electro-mechanical fields (Sladek 2007a), crack analysis in two-dimensional (2-D) and three-dimensional (3-D) axisymmetric piezo-electric solids with continuously varying material properties (Sladek 2007b) and the solution of boundary value problems for coupled thermo-electro-mechanical fields (Sladek 2007c).

The Local Boundary Integral Equation method (LBIE) with moving least square and polynomial radial basis function (RBF) has been developed by Sladek et al (2004, 2005a, 2006b) for boundary value problems in anisotropic non-homogeneous media i.e. functionally graded materials. Both methods (MLPG and LBIE) are meshless, as no domain/boundary meshes are required in these two approaches. However, Galerkin-base meshless methods, except for MLGP presented by Atluri (2004) still include several awkward implementation features such as numerical integrations in the local domain. A comprehensive review of meshless methods can be found in the book by Atluri (2004).

Using the finite element method, we are able to evaluate the displacements and stresses in each element by its nodal values of displacement. In addition, the material properties such as Young's modulus and Poisson ratio are treated as constants in each element. Apparently the stresses are not continuous crossing each element, despite the displacements being continuous everywhere. Hence, these discontinuities of stress and material properties in the field are considered to be one of the

reasons that affect the accuracy of numerical simulation. For instance, to achieve high accuracy around a sharp corner or in front of the crack tips, high density of element or special elements must be introduced in the local region by FEM. The application of meshless method to fracture mechanics i.e. the evaluation of stress intensity factors at crack tips and analysis of crack growth were demonstrated by Fleming et al (1997) and Rao et al (2001) using enriched basis function with moving least square (MLS) interpolation. However, this method is quite expensive computationally, because the derivative of the shape function is complicated at every Gauss integral point. Functionally graded materials (FGM) have continuous non-homogeneous material properties and have been widely used in manufactory industries such as civil engineering and the aerospace industry. To deal with crack problems in functionally graded materials for two-dimensional elasticity, Sladek et al (2004) presented a local integral equation formulation and a new equivalent domain integral to evaluate stress intensity factors. In this paper, the element-free Galerkin method is presented with compactly supported enriched radial basis function (RBF) interpolation. Following the same way to derive system equations for FEM, the stiffness matrix is determined by the principle of potential energy variation using enriched RBF interpolations. It can be found that the stiffness matrix of the system is still symmetric and strip-diagonally distributed. Therefore, this method can be easily combined with FEM. Numerical results have been given for a rectangular sheet and a circular plate with central and edge cracks. Comparisons have been made with numerical results by Sladek et al (2004) using LBIE. This method can be easily extended to dynamic fracture mechanics with all types of functionally graded materials.

2 Variation of potential energy

In the case of a homogeneous anisotropic and linear elasticity, we have a relation between the stress and strain by Hooke's law

$$\sigma_{ij}(\mathbf{x}) = C_{ijkl}(\mathbf{x})\epsilon_{kl}(\mathbf{x}) = C_{ijkl}(\mathbf{x})u_{k,l}(\mathbf{x}), \quad (1)$$

where $\varepsilon_{kl} = (u_{k,l} + u_{l,k})/2$, and C_{ijkl} denotes the elasticity tensor, which has the following symmetries

$$C_{ijkl} = C_{jikl} = C_{klij}. \quad (2)$$

For a homogeneous isotropic solid, we have

$$C_{ijkl}(\mathbf{x}) = \lambda(\mathbf{x})\delta_{ij}\delta_{kl} + \mu(\mathbf{x})(\delta_{ik}\delta_{jl} + \delta_{il}\delta_{jk}) \quad (3)$$

where λ and μ are the Lamé's constants, which are the function of coordinate for the continuous non-homogeneity. For the isotropic plane stress state, Hooke's law can also be written in matrix form, as

$$\boldsymbol{\sigma} = \begin{Bmatrix} \sigma_{11} \\ \sigma_{11} \\ \sigma_{11} \end{Bmatrix} = \mathbf{D}(\mathbf{x}) \begin{Bmatrix} \varepsilon_{11} \\ \varepsilon_{22} \\ \varepsilon_{12} \end{Bmatrix} = \mathbf{D}(\mathbf{x})\boldsymbol{\varepsilon} \quad (4)$$

where

$$\mathbf{D}(\mathbf{x}) = \frac{E(\mathbf{x})}{1-\nu(\mathbf{x})^2} \begin{bmatrix} 1 & \nu(\mathbf{x}) & 0 \\ \nu(\mathbf{x}) & 1 & 0 \\ 0 & 0 & \frac{1-\nu(\mathbf{x})}{2} \end{bmatrix} \quad (5)$$

in which, $E(\mathbf{x})$ is the Young's modulus and $\nu(\mathbf{x})$ the Poisson ratio. For the plane-strain state, we need to change the Young's modulus and the Poisson ratio by $E/(1-\nu^2)$ and $\nu/(1-\nu)$ in (5) respectively. Consider the domain Ω enclosed by the boundary Γ , we have the total potential energy for the plane stress

$$\Pi = U - W \quad (6)$$

where the initial elastic strain energy

$$\begin{aligned} U &= \frac{1}{2} \int_{\Omega} \boldsymbol{\sigma}^T(\mathbf{y})\boldsymbol{\varepsilon}(\mathbf{y})d\Omega(\mathbf{y}) \\ &= \frac{1}{2} \int_{\Omega} \boldsymbol{\varepsilon}^T(\mathbf{y})\mathbf{D}(\mathbf{y})\boldsymbol{\varepsilon}(\mathbf{y})d\Omega(\mathbf{y}) \end{aligned} \quad (7)$$

and the external energy, i.e. the sum of contributions from known interior and boundary forces

$$W = \int_{\Omega} \mathbf{u}^T(\mathbf{y})\mathbf{b}(\mathbf{y})d\Omega(\mathbf{y}) + \int_{\Gamma} \mathbf{u}^T(\mathbf{y})\mathbf{t}(\mathbf{y})d\Gamma(\mathbf{y}) \quad (8)$$

where $\mathbf{b} = \{b_1, b_2\}^T$ is the body force vector, $\mathbf{t} = \{t_1, t_2\}^T$, in which $t_i = \sigma_{ij}n_j$ is the vector of traction on the boundary and n_i denotes the component of a unit outward normal vector. We assume that the displacements $\mathbf{u}(\mathbf{y})$ at the point \mathbf{y} can be approximated by the nodal values in a local domain (support domain), as shown in Figure 1 as

$$\begin{aligned} u_i(\mathbf{y}) &= \sum_{k=1}^{n(\mathbf{y})} \phi_k(\mathbf{y}, \mathbf{x}_k) \hat{u}_i^k = \bar{\boldsymbol{\Phi}}(\mathbf{y}, \mathbf{x}) \hat{\mathbf{u}}_i \\ \bar{\boldsymbol{\Phi}}(\mathbf{y}, \mathbf{x}) &= \{\phi_1(\mathbf{y}, \mathbf{x}_1), \phi_2(\mathbf{y}, \mathbf{x}_2), \dots, \phi_{n(\mathbf{y})}(\mathbf{y}, \mathbf{x}_{n(\mathbf{y})})\} \\ \hat{\mathbf{u}}_i &= \{\hat{u}_i^1, \hat{u}_i^2, \dots, \hat{u}_i^{n(\mathbf{y})}\}^T, \quad i = 1, 2 \end{aligned} \quad (9)$$

$\hat{u}_i(\mathbf{x})$ is the nodal values at point $\mathbf{x}_k = \{x_1^{(k)}, x_2^{(k)}\}$, $k = 1, 2, \dots, n(\mathbf{y})$, ϕ_k the shape function and $n(\mathbf{y})$ the total number of nodes in the local domain, named as the supported domain. For the plane-stress problem, we can rearrange the above relation as follows

$$\begin{aligned} \mathbf{u}(\mathbf{y}) &= \{u_1, u_2\}^T = \boldsymbol{\Phi}(\mathbf{y}, \mathbf{x}) \hat{\mathbf{u}} \\ \boldsymbol{\Phi}(\mathbf{y}, \mathbf{x}) &= \begin{bmatrix} \bar{\boldsymbol{\Phi}} & 0 \\ 0 & \boldsymbol{\Phi} \end{bmatrix} \\ &= \begin{bmatrix} \phi_1 & 0 & \phi_2 & 0 & \dots & \phi_{n(\mathbf{y})} & 0 \\ 0 & \phi_1 & 0 & \phi_2 & \dots & 0 & \phi_{n(\mathbf{y})} \end{bmatrix} \\ \hat{\mathbf{u}} &= \{\hat{u}_1^1, \hat{u}_2^1, \hat{u}_1^2, \hat{u}_2^2, \dots, \hat{u}_1^{n(\mathbf{y})}, \hat{u}_2^{n(\mathbf{y})}\}^T \end{aligned} \quad (10)$$

Therefore, the relationship between strains and displacements is given by

$$\begin{aligned} \boldsymbol{\varepsilon}(\mathbf{y}) &= \begin{bmatrix} \frac{\partial \phi_1}{\partial x} & 0 & \frac{\partial \phi_2}{\partial x} & 0 & \dots & \frac{\partial \phi_{n(\mathbf{y})}}{\partial x} & 0 \\ 0 & \frac{\partial \phi_1}{\partial y} & 0 & \frac{\partial \phi_2}{\partial y} & \dots & 0 & \frac{\partial \phi_{n(\mathbf{y})}}{\partial y} \\ \frac{\partial \phi_1}{\partial y} & \frac{\partial \phi_1}{\partial x} & \frac{\partial \phi_2}{\partial y} & \frac{\partial \phi_2}{\partial x} & \dots & \frac{\partial \phi_{n(\mathbf{y})}}{\partial y} & \frac{\partial \phi_{n(\mathbf{y})}}{\partial x} \end{bmatrix} \hat{\mathbf{u}} \\ &= \mathbf{B}(\mathbf{y}) \hat{\mathbf{u}}. \end{aligned} \quad (11)$$

To obtain the system equations in terms of nodal displacement, the minimum value principle of total potential energy with respect to each nodal displacement is considered and it gives

$$\delta \Pi = \delta U - \delta W = 0 \quad (12)$$

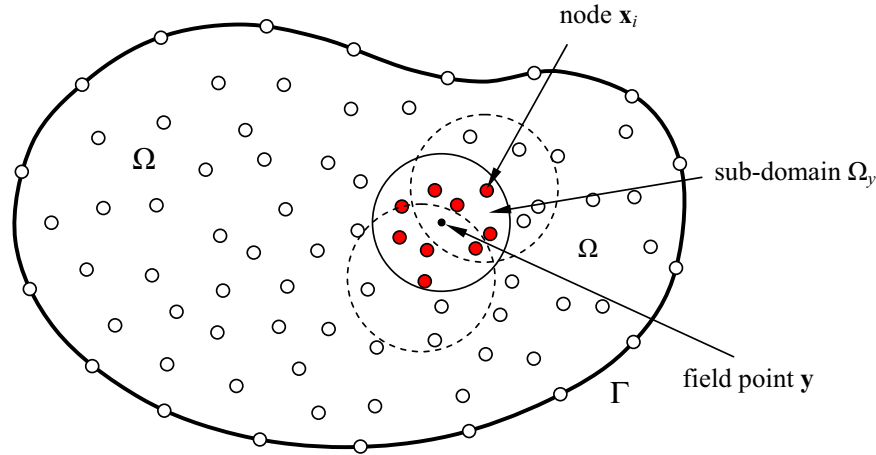


Figure 1: Sub-domain Ω_y for RBF interpolation of the field point \mathbf{y} and support domains.

Inserting the relationships $\mathbf{u} = \Phi \hat{\mathbf{u}}$, $\boldsymbol{\varepsilon} = \mathbf{B} \hat{\mathbf{u}}$ and $\boldsymbol{\sigma} = \mathbf{D} \boldsymbol{\varepsilon}$ into (12) yields $2 \times N$ linear algebraic equations in global coordinate:

$$[\mathbf{K}]_{2N \times 2N} \hat{\mathbf{u}}_{2N} + [\mathbf{M}]_{2N \times 2N} \hat{\mathbf{u}} = \mathbf{f}_{2N} \quad (13)$$

where N is the total number of nodes in the domain Ω . The stiffness matrix becomes:

$$\mathbf{K} = \int_{\Omega} \mathbf{B}^T(\mathbf{x}, \mathbf{y}) \mathbf{D}(\mathbf{y}) \mathbf{B}(\mathbf{x}, \mathbf{y}) d\Omega(\mathbf{y}) \quad (14)$$

$$\mathbf{M} = \rho \int_{\Omega} \Phi^T(\mathbf{x}, \mathbf{y}) \Phi(\mathbf{x}, \mathbf{y}) d\Omega(\mathbf{y})$$

and the nodal force vector is

$$\mathbf{f} = \int_{\Omega} \Phi^T(\mathbf{x}, \mathbf{y}) \mathbf{b}(\mathbf{y}) d\Omega(\mathbf{y}) + \int_{\Gamma_{\sigma}} \Phi^T(\mathbf{x}, \mathbf{y}) \mathbf{t}(\mathbf{y}) d\Gamma(\mathbf{y}) \quad (15)$$

where Γ_{σ} denotes the boundary on which the traction is given. For two concentrated forces acting at the node i , we can determine the nodal force vector directly by

$$\mathbf{f}_i = \{F_1^i, F_2^i\}^T \quad (16)$$

where F_1 and F_2 denote the values of concentrated forces either on the boundary (externally applied force) or in the domain (inner body force). Therefore the loads, including the boundary loads and the body forces can be simplified to nodal forces in the same way as FEM. Thus, the domain and

the boundary integrals in (15) can be evaluated directly. It is worth noticing that by the finite element method, the displacements at point \mathbf{y} can be determined approximately by the nodal values of its own element and the number of nodes depends on the element type. For instance, the number of nodes is 3 for triangle element and is 4 for rectangular element respectively. From the interpolation point of view, the accuracy of MLS and RBF should be higher, since more nodes are considered in the support domain.

3 The approximation schemes

The multiquadric RBF was introduced by Hardy (1971) for the interpolation of topographical surfaces. Since all radial basis functions are defined globally, the resulting matrix for interpolation is dense and can be highly ill-conditioned, particularly for a large number of interpolation points. It poses serious stability problems and is also computationally inefficient.

A sub-domain Ω_y , as shown in Figure 1 is the neighbourhood of a point \mathbf{y} and is also called the support domain to an arbitrary point \mathbf{y} . The distribution of function u in the sub-domain Ω_y over a number of randomly distributed nodes $\{\mathbf{x}_i\}$, $i = 1, 2, \dots, n(\mathbf{y})$ can be interpolated at the point \mathbf{y} by

$$u(\mathbf{y}) = \sum_{i=1}^{n(\mathbf{y})} R_i(\mathbf{y}, \mathbf{x}_i) a_i = \mathbf{R}^T(\mathbf{y}, \mathbf{x}) \mathbf{a}(\mathbf{y}) \quad (17)$$

where $\mathbf{R}^T(\mathbf{y}, \mathbf{x}) =$

$\{R_1(\mathbf{y}, \mathbf{x}), R_2(\mathbf{y}, \mathbf{x}), \dots, R_{n(\mathbf{y})}(\mathbf{y}, \mathbf{x})\}$ is a set of radial basis functions centred at the point \mathbf{y} , $\{a_k\}_{k=1}^{n(\mathbf{y})}$ are the unknown coefficients to be determined. To capture the singular stresses in front of the crack tip, the enriched radial basis function has been selected to be the following

$$R_k(\mathbf{y}, \mathbf{x}) = R(\mathbf{y} - \mathbf{x}_k) + Q(\mathbf{y}) = \sqrt{c^2 + |\mathbf{y} - \mathbf{x}_k|^2} + (\beta + \sqrt{r}e^{-\alpha r}) \quad (18)$$

where $r = |\mathbf{y} - \mathbf{y}_c|$; α , β and c are three free parameters; $\mathbf{y}_c (y_1^{(c)}, y_2^{(c)})$ denotes the crack tip. Also we select $c = b$ (b is the specified length such as the width of the rectangular plate or the radius of the circular disk etc) in this paper. To deal with mixed-mode fracture problems, generally the sub-region technique used by the boundary element method and the mesh-free method should be employed. Due to the discontinuities of displacement and traction between upper and lower crack surfaces, the traditional support domain such as a circular domain is not valid for mixed-mode problems. In this paper, a C-shaped support domain is adopted for a collocation point, which is near to the crack surfaces. Four cases are shown in Figure 2, where the straight line CB is the extension of the line connecting points A (collocation \mathbf{y} ,) and C (crack tip \mathbf{y}_c). Therefore, the discontinuity of displacement can be described using the radial basis functions.

For the interpolation strategy in (18) for RBF, a linear system for the unknown coefficients \mathbf{a} is obtained by

$$\mathbf{R}_0 \mathbf{a} = \hat{\mathbf{u}} \quad (19)$$

where coefficient matrix

$$\mathbf{R}_0 = \begin{bmatrix} R_1(\mathbf{x}_1, \mathbf{x}_1) & R_2(\mathbf{x}_1, \mathbf{x}_2) & \dots \\ R_1(\mathbf{x}_2, \mathbf{x}_1) & R_2(\mathbf{x}_2, \mathbf{x}_2) & \dots \\ \vdots & \vdots & \dots \\ \vdots & \vdots & \dots \\ R_1(\mathbf{x}_{n(\mathbf{y})}, \mathbf{x}_1) & R_2(\mathbf{x}_{n(\mathbf{y})}, \mathbf{x}_2) & \dots \end{bmatrix}$$

$$\begin{bmatrix} R_{n(\mathbf{y})}(\mathbf{x}_1, \mathbf{x}_{n(\mathbf{y})}) \\ R_{n(\mathbf{y})}(\mathbf{x}_2, \mathbf{x}_{n(\mathbf{y})}) \\ \vdots \\ \vdots \\ R_{n(\mathbf{y})}(\mathbf{x}_{n(\mathbf{y})}, \mathbf{x}_{n(\mathbf{y})}) \end{bmatrix} \quad (20)$$

As RBFs are positive definite, the matrix \mathbf{R}_0 is assured to be invertible. Therefore, we can obtain the vector of unknowns from (19)

$$\mathbf{a} = \mathbf{R}_0^{-1}(\mathbf{x}) \hat{\mathbf{u}}(\mathbf{x}) \quad (21)$$

So that the approximation $u(\mathbf{y})$ can be represented at domain point \mathbf{y} by

$$u(\mathbf{y}) = \mathbf{R}^T(\mathbf{y}, \mathbf{x}) \mathbf{R}_0^{-1}(\mathbf{x}) \hat{\mathbf{u}}(\mathbf{x}) = \bar{\Phi}(\mathbf{y}, \mathbf{x}) \hat{\mathbf{u}} = \sum_{k=1}^{n(\mathbf{y})} \phi_k \hat{u}_k \quad (22)$$

where the nodal shape function are defined by

$$\bar{\Phi}(\mathbf{y}, \mathbf{x}) = \mathbf{R}^T(\mathbf{y}, \mathbf{x}) \mathbf{R}_0^{-1}(\mathbf{x}) \quad (23)$$

It is worth noticing that the shape function depends uniquely on the distribution of scattered nodes within the support domain and has the Kronecker Delta property. As the inverse matrix of the coefficients $\mathbf{R}_0^{-1}(\mathbf{x})$ depends only on the distribution of nodes \mathbf{x}_i in the support domain, it is simple to evaluate the partial derivatives of the shape function with respect to coordinates. From (22), we have

$$u_{,k}(\mathbf{y}) = \frac{\partial u(\mathbf{y})}{\partial y_k} = \bar{\Phi}_{,k}(\mathbf{y}, \mathbf{x}) \hat{\mathbf{u}} = \sum_{i=1}^{n(\mathbf{y})} \phi_{i,k} \hat{u}_i \quad (24)$$

where

$$\begin{aligned} \bar{\Phi}_{,k}(\mathbf{y}, \mathbf{x}) &= \mathbf{R}_{,k}^T(\mathbf{y}, \mathbf{x}) \mathbf{R}_0^{-1}(\mathbf{x}) \\ &= [R_{1,k}(\mathbf{y}, \mathbf{x}), R_{2,k}(\mathbf{y}, \mathbf{x}), \dots, R_{n(\mathbf{y}),k}(\mathbf{y}, \mathbf{x})] \mathbf{R}_0^{-1}(\mathbf{x}) \end{aligned} \quad (25)$$

in which

$$R_{i,k}(\mathbf{y}, \mathbf{x}_i) = \frac{y_k - x_k^{(i)}}{\sqrt{c^2 + |\mathbf{y} - \mathbf{x}_i|^2}} + \frac{y_k - y_k^{(c)}}{r} \left(\frac{1}{2\sqrt{r}} - \alpha \right) e^{-\alpha r}. \quad (26)$$

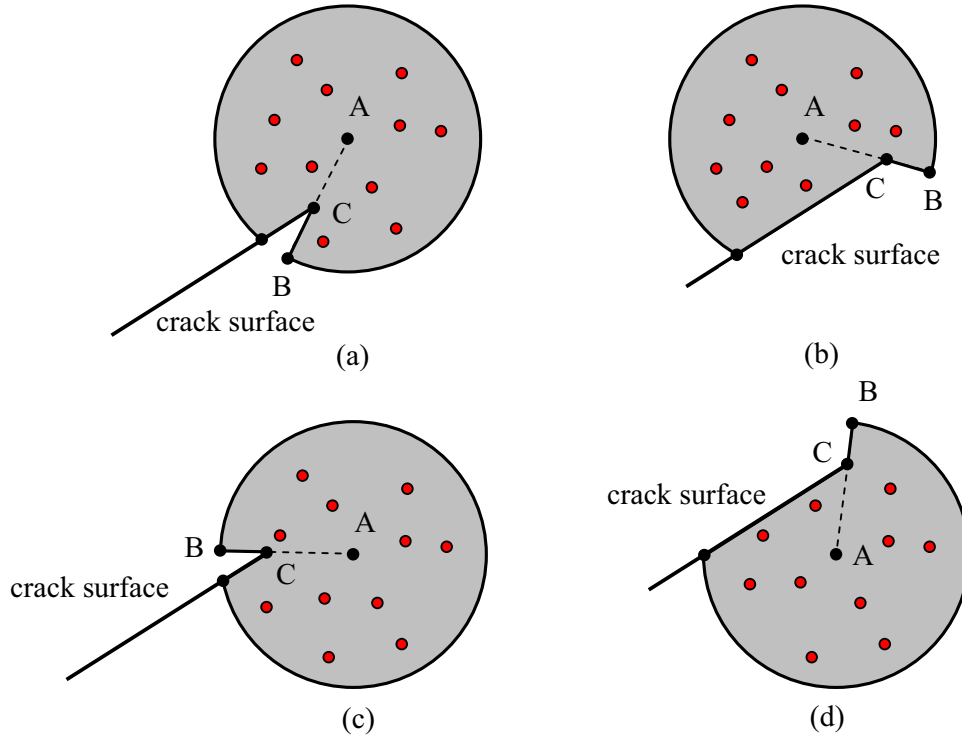


Figure 2: Local support domains near to the crack surfaces.

Therefore, the strains are of singularity with $1/\sqrt{r}$ near the crack tip, as expected. In order to guarantee a unique solution of the interpolation problem, a polynomial term should be added to the interpolation in Eq.(18) as

$$u(\mathbf{y}) = \sum_{k=1}^{n(\mathbf{y})} R_k(\mathbf{y}, \mathbf{x}) a_k + \sum_{j=1}^t P_j(\mathbf{y}) b_j \quad (27)$$

$$= \mathbf{R}_0(\mathbf{y}, \mathbf{x}) \mathbf{a} + \mathbf{P}(\mathbf{y}) \mathbf{b}$$

along with the constraints

$$\sum_{j=1}^t P_k(\mathbf{x}_j) a_j = 0, \quad 1 \leq k \leq t \quad (28)$$

where $\{P_k\}_{k=1}^t$ is a basis for P_{m-1} , the set of d-variate polynomials of degree $\leq m-1$ and

$$t = \binom{m+d-1}{d} \quad (29)$$

is the dimension of P_{m-1} . A set of linear equations can be written in the matrix form as

$$\mathbf{R}_0 \mathbf{a} + \mathbf{P}^T \mathbf{b} = \hat{\mathbf{u}}, \quad \mathbf{P} \mathbf{a} = \mathbf{0} \quad (30)$$

where the matrix

$$P(\mathbf{x}) = \begin{bmatrix} P_1(x_1) & P_2(x_1) & \dots & P_t(x_1) \\ P_1(x_2) & P_2(x_2) & \dots & P_t(x_2) \\ \vdots & \vdots & \ddots & \vdots \\ P_1(x_n) & P_2(x_n) & \dots & P_t(x_n) \end{bmatrix} \quad (31)$$

Solving equations in Eq.(31) gives

$$\mathbf{b} = (\mathbf{P}^T \mathbf{R}_0^{-1} \mathbf{P})^{-1} \mathbf{P}^T \mathbf{R}_0^{-1} \hat{\mathbf{u}}, \quad (32)$$

$$\mathbf{a} = \mathbf{R}_0^{-1} \left[\mathbf{I} - \mathbf{P} (\mathbf{P}^T \mathbf{R}_0^{-1} \mathbf{P})^{-1} \mathbf{P}^T \mathbf{R}_0^{-1} \right] \hat{\mathbf{u}}$$

where \mathbf{I} denotes the diagonal unit matrix. It is clear that the coefficients \mathbf{a} and \mathbf{b} are functions of nodal coordinate \mathbf{x} in the support domain. In addition, the accuracy has been shown to be the same by using RBF with/without these polynomials. Therefore, the shape functions with radial basis function are selected by Eq.(23) for simplicity in the following analysis.

4 Numerical process to evaluate stiffness matrix

To determine the stiffness matrix \mathbf{K} in (13), a domain integral in (14) over the domain Ω should be calculated numerically. For the convenience of analysis, we assume that the domain can be divided into M rectangular sub-regions (cells). For the irregular shape of the integral sub-domain, coordinate transformation i.e. technique of coordinate transformation should be introduced. A two-dimensional domain integral over a rectangular area can be evaluated by the Gaussian integral formula

$$\iint_A f(x_1, x_2) dx_1 dx_2 \approx A \sum_{i=1}^L w_i f(x_1^{(i)}, x_2^{(i)}) \quad (33)$$

where w_i denotes the weight of integral, L the number of integral Gaussian points and $(x_1^{(i)}, x_2^{(i)})$ is the coordinate of Gaussian points, as shown in Figure 2. The matrix of stiffness can be rearranged by four-Gaussian-points scheme as

$$\begin{aligned} \mathbf{K}(\mathbf{x}) &= \int_{\Omega} \mathbf{B}^T(\mathbf{x}, \mathbf{y}) \mathbf{D}(\mathbf{y}) \mathbf{B}(\mathbf{x}, \mathbf{y}) d\Omega(\mathbf{y}) \\ &= \sum_{m=1}^M \sum_{l=1}^4 \frac{A_m}{4} \mathbf{B}^T(\mathbf{x}, \mathbf{y}_m^{(l)}) \mathbf{D}(\mathbf{y}_m^{(l)}) \mathbf{B}(\mathbf{x}, \mathbf{y}_m^{(l)}) \\ &= \sum_{m=1}^M \sum_{l=1}^4 \Delta \mathbf{K}_l^m \end{aligned} \quad (34)$$

where coefficients w_l are given by

$$\begin{aligned} \mathbf{y}_m^{(1,2,3,4)} &= \left(y_1^m \pm \sqrt{\frac{1}{3}} h_1, y_2^m \pm \sqrt{\frac{1}{3}} h_2 \right), \\ w_{1,2,3,4} &= \frac{1}{4}, \end{aligned} \quad (35)$$

in which $\mathbf{y}_m(y_1^m, y_2^m)$ presents the centre of the sub integral domain with area A_m (rectangular), h_1 and h_2 are the half lengths of width and height respectively and $A_m = 4h_1h_2$. For each Gaussian point \mathbf{y}_l , the elements in the sub-matrix $\Delta \mathbf{K}_l^m$ can be simplified for the plane-stress state as

$$\Delta \mathbf{K}_l^m =$$

$$\begin{aligned} \frac{A_m E(\mathbf{y}_l)}{4[1 - \nu^2(\mathbf{y}_l)]} & \left[\begin{array}{c} \frac{\partial \phi_i}{\partial y_1} \frac{\partial \phi_j}{\partial y_1} + \frac{1 - \nu(\mathbf{y}_l)}{2} \frac{\partial \phi_i}{\partial y_2} \frac{\partial \phi_j}{\partial y_2} \\ \nu(\mathbf{y}_l) \frac{\partial \phi_i}{\partial y_2} \frac{\partial \phi_j}{\partial y_1} + \frac{1 - \nu(\mathbf{y}_l)}{2} \frac{\partial \phi_i}{\partial y_1} \frac{\partial \phi_j}{\partial y_2} \\ \nu(\mathbf{y}_l) \frac{\partial \phi_i}{\partial y_1} \frac{\partial \phi_j}{\partial y_2} + \frac{1 - \nu(\mathbf{y}_l)}{2} \frac{\partial \phi_i}{\partial y_2} \frac{\partial \phi_j}{\partial y_1} \\ \frac{\partial \phi_i}{\partial y_2} \frac{\partial \phi_j}{\partial y_2} + \frac{1 - \nu(\mathbf{y}_l)}{2} \frac{\partial \phi_i}{\partial y_1} \frac{\partial \phi_j}{\partial y_1} \end{array} \right]_{ij} \\ &= \begin{bmatrix} a'_{11} & a'_{12} \\ a'_{21} & a'_{22} \end{bmatrix}_{ij} \end{aligned} \quad (36)$$

where i and j denote the number of nodes in the local support domain centred at \mathbf{y}_l , $\phi_i = \phi_i(\mathbf{y}_l, \mathbf{x})$, $i, j=1, 2, \dots, n(\mathbf{y}_l)$. These four values in (37) should be added to the global stiffness matrix \mathbf{K} , i.e. to the elements $k_{2I-1, 2J-1}, k_{2I-1, 2J}, k_{2I, 2J-1}$ and $k_{2I, 2J}$ respectively, where I and J denote the numbers in the global coordinate for the node i and j in the local support domain. For the stiffness matrix \mathbf{K} in (35), the integral function has strong singularity $1/r$ around the crack tip, due to an enriched radial base function. Therefore, we need to use coordinate transformation to cancel that singularity in the sub-region integrals near the crack tip. For example, the sub-region (two squares) needs to be divided into four triangular sub-domains and each sub-domain is transformed into a square as shown in Figure 3. The transformations can be presented by, [see Aliabadi (2002)]

Triangular I: $y_1 = \xi_1$ and $y_2 = \frac{1}{2}[(1 + \xi_1)\xi_2 - (1 - \xi_1)]$; $J_c = \frac{1}{2}(1 + \xi_1)$

Triangular II: $y_1 = \frac{1}{2}[(1 + \xi_1)\xi_2 - (1 - \xi_1)]$ and $y_2 = \xi_1$; $J_c = \frac{1}{2}(1 + \xi_1)$

Triangular III: $y_1 = \frac{1}{2}[(1 + \xi_2)\xi_1 + (1 - \xi_2)]$ and $y_2 = \xi_2$; $J_c = \frac{1}{2}(1 + \xi_2)$

Triangular IV: $y_1 = -\xi_2$ and $y_2 = -\frac{1}{2}[(1 + \xi_2)\xi_1 + (1 - \xi_2)]$; $J_c = \frac{1}{4}(1 + \xi_2)$

Thus, the integral with a strong singularity at $\mathbf{y}_c(-1, -1)$ can be written as

$$\begin{aligned} & \int_{-1}^1 \int_{-1}^1 \frac{F(y_1, y_2)}{r} dy_1 dy_2 = \\ & \int_{-1}^1 \int_{-1}^1 \frac{F(y_1, y_2)}{r} J_c^I(\xi_1) d\xi_1 d\xi_2 \\ & + \int_{-1}^1 \int_{-1}^1 \frac{F(y_1, y_2)}{r} J_c^{II}(\xi_2) d\xi_1 d\xi_2 \end{aligned}$$

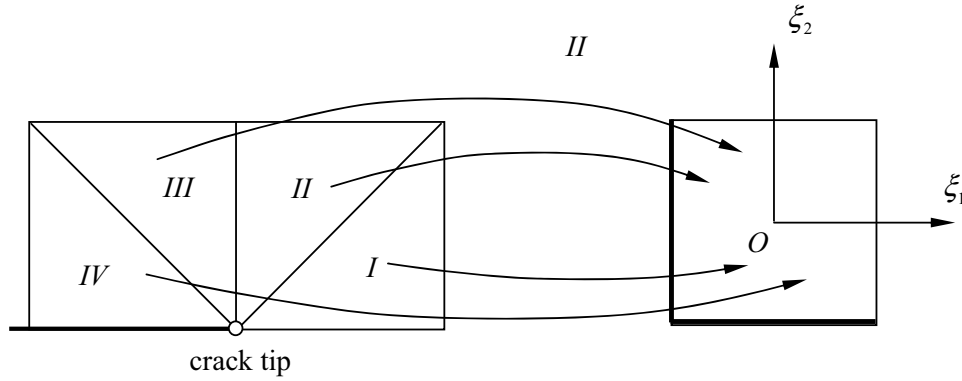


Figure 3: Transformation of a triangle to a square.

$$\begin{aligned}
 & + \int_{-1}^1 \int_{-1}^1 \frac{F(y_1, y_2)}{r} J_c^{III}(\xi_1) d\xi_1 d\xi_2 \\
 & + \int_{-1}^1 \int_{-1}^1 \frac{F(y_1, y_2)}{r} J_c^{IV}(\xi_2) d\xi_1 d\xi_2 \quad (37)
 \end{aligned}$$

in which the Jacobian factors cancel out the $1/r$ singularity successfully.

Obviously the system stiffness matrix \mathbf{K} is symmetric and has a diagonal strip distribution, which is similar to the stiffness matrix for the finite element method. As there are more nodes in the local support domain than FEM (one element), it is believed that more accurate stress and strain (continuous) solutions should be obtained. The implementation of this method can be carried out according to the following routines, which are similar to the meshless method discussed by Atluri (2004):

Choose a finite number of nodes N in the domain Ω and on the boundary Γ of the given physical domain; choose interpolation scheme such as MLS or RBF,

Select the size and shape of local support domain or the minimum number in the support domain Ω_y

Divide the domain Ω into segments and choose the shape of integral sub-domain

Loop over the integral in the sub domain m ($m=1, 2, \dots, M$) centred at \mathbf{y}_m

Loop over the integral Gaussian points \mathbf{y}_l ($l=1, 2, 3, 4$) in the sub-domain,

Loop over all nodes in the support domain (i, j) ;

Calculate the shape function $\phi_i(\mathbf{y}, \mathbf{x}_i)$ and first derivative $\phi_{i,k}(\mathbf{y}, \mathbf{x}_i)$;

Evaluate the elements $\Delta \mathbf{K}_l^m = [a_{kl}^l]_{ij}$ with enrichment at crack tip;

Assemble the system stiffness matrix $\mathbf{K}_{(I,J)}$;

End the node loop in the local domain,

End the Gaussian point loop,

End the sub-domain of integral loop,

Introduce the displacement boundary condition and modify the system equation,

Solve the linear equations for the nodal values,

Calculate the stresses and unknown variables by using the interpolations in the local support domain.

In addition, the width of the strip in the system matrix depends on the size of the support domain or on the number of nodes in the support region. Therefore, the combination of element-free Galerkin method with the finite element method can be realised easily. The mixed mode stress intensity factors are evaluated using the crack opening displacements (COD) near the crack tip \mathbf{x}_c , for plane-stress state by

$$\begin{aligned}
 K_I &= \frac{E(\mathbf{y}_c)}{8} \sqrt{\frac{2\pi}{r_0}} \Delta u_2, & \Delta u_2 &= u_2^+ - u_2^- \\
 K_{II} &= \frac{E(\mathbf{y}_c)}{8} \sqrt{\frac{2\pi}{r_0}} \Delta u_1, & \Delta u_1 &= u_1^+ - u_1^-
 \end{aligned} \quad (38)$$

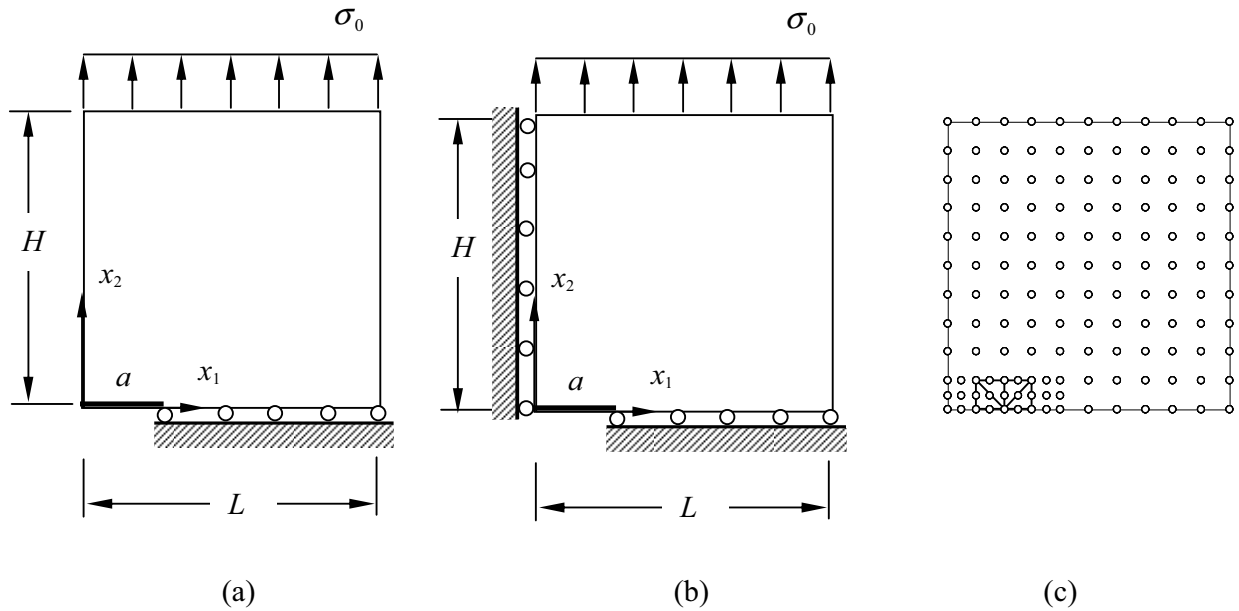


Figure 4: Square plate with a central crack ($H = L$) under tensile load σ_0 : (a) a half of the plate with edge crack; (b) a quarter of the plate with central crack; (c) uniformly distributed nodes (138 nodes).

5 Numerical examples

5.1 A rectangular plate with an edge crack

A rectangular plate with width L and height $2L$ containing an edge crack of length $a=0.2L$ is considered. Due to the symmetry, half of the plate is analyzed, as shown in Figure 4 (a). Plane-strain state is assumed and Poisson ratio $\nu=0.3$ in the domain (constant) for all examples. Densities of node (11×11) and (21×21) are selected in this example and thus, 138 and 458 nodes in total are uniformly distributed respectively in the domain and on the boundary, including extra nodes in two special cells (integral with singularity). Figure 4(c) shows the uniform distribution for 138 nodes. The grid of sub-region for domain integral is selected as (10×10) and therefore the sub-region number $M=100$ in Figure 4(c). Uniform stress σ_0 is applied on the top of the plate. The support domain is selected as a circle of radius d_y centered at the field point \mathbf{y} , which is determined such that the minimum number of nodes in the sub-domain $n(\mathbf{y}) \geq N_0$, here $N_0 = 10$ for all of the following examples. However, we noticed that for a large number of support nodes in the sub-domain, the interpolation will become unstable for RBF interpolations, due to the computa-

tional precision of FORTRAN. The Young's modulus is graded along the crack exponentially as $E(x_1) = E_1 \exp(\delta x_1/L)$, where $\delta = \ln(E_2/E_1)$. E_1 and E_2 denote the Young's modulus when $x_1 = 0$ and L respectively. In addition, free parameters $\alpha = 1/L$, $\beta = L$, $c = L$ in (18) and $r_0 = 2\Delta$ in all examples, where Δ is the gap between two nodes in front of the crack tip. The optimization for these parameters selection was discussed in detail by Wen et al (2007) for isotropic materials. Numerical results of normalized stress intensity factor $K_I/\sigma_0\sqrt{\pi a}$ for two groups of different mesh density are shown in Table 1. Also, the results given by Sladek et al (2004) and Kim et al (2002) are presented in the table for comparisons. It can be seen that for higher density of the node distribution, the percentage of relative error is less than 5%.

5.2 A single centred crack in rectangular plate under tensile load

A square plate of width $2L$ containing a centred crack of half length $a = 0.2L$ subjected to a uniform shear load σ_0 on the top and the bottom is studied. Due to the symmetry, a quarter of the plate is considered, as shown in Figure 4(b). The same distribution format of nodes in Example

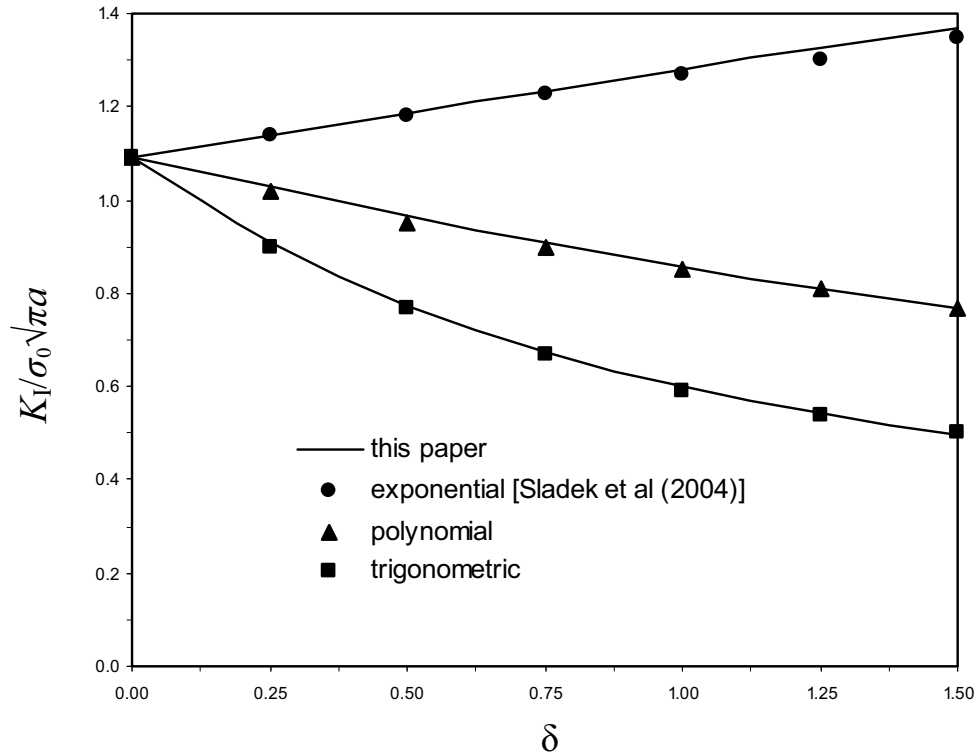


Figure 5: Normalized stress intensity factors for continuous non-homogeneity.

Table 1: SIFs $K_I/\sigma_0\sqrt{\pi a}$ for an edge crack under tensile load

E_2/E_1	This paper		Sladek et al (2005)	Kim et al (2002)
	$N_{\text{total}} = 138$	$N_{\text{total}} = 458$		
0.1	1.1643	1.2502	1.3198	1.284
0.2	1.3057	1.3498	1.3950	1.390
1.0	1.3432	1.3278	1.3520	1.358
5.0	1.1406	1.1022	1.1385	1.132
10.0	1.0195	0.9785	1.0255	1.003

5.1 is selected ($N_{\text{total}} = 458$). To compare with numerical results given by Sladek et al (2004), three kinds of variation of the gradation function with respect to x_2 are considered too i.e. (a) $E(x_2) = E_0 [\cos(\delta x_2/L) + 5 \exp(-\delta x_2/L)]^2$; (b) $E(x_2) = E_0 (1 + \delta x_2/L)^2$; (c) $E(x_2) = E_0 [\cos(\delta x_2/L) + 3 \sin(\delta x_2/L)]^2$. Figure 5 shows the variations of normalized stress intensity factor $K_I/\sigma_0\sqrt{\pi a}$ against parameter δ . Excellent agreement with the solutions by Sladek et al (2004) is achieved.

5.3 A circular disk with a central crack under tension

A circular disk of radius R containing a central crack of half length $a = 0.4R$ subjected to a uniform tension σ_0 on the boundary along the normal direction is shown in Figure 6(a). A quarter of the disk shown in Figure 6(b) is analyzed. In this model, we consider two densities of the uniformly distributed nodes in the domain, i.e. $N_{\text{total}} = 118$ and 370 respectively. Three kinds of variation of the gradation function are considered i.e. the Young's modulus (a) $E(x_1) = E_1 \exp(\delta x_1/R)$; (b) $E(x_2) = E_1 \exp(\delta x_2/R)$ and (c) $E(x_1, x_2) =$

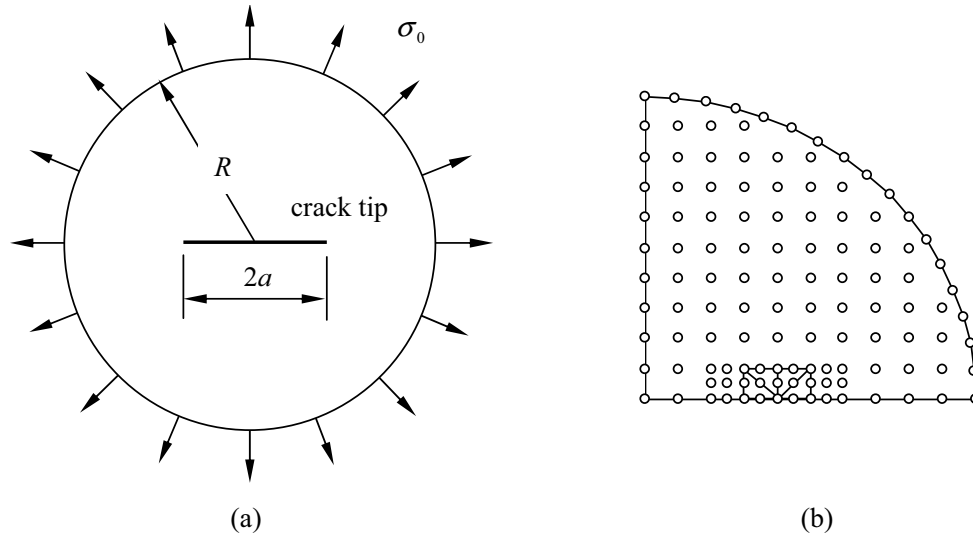


Figure 6: A circular disk of radius R with a central crack of length $2a$ subjected to uniform load σ_0 on the boundary: (a) geometry; (b) distribution of nodes (118 nodes).

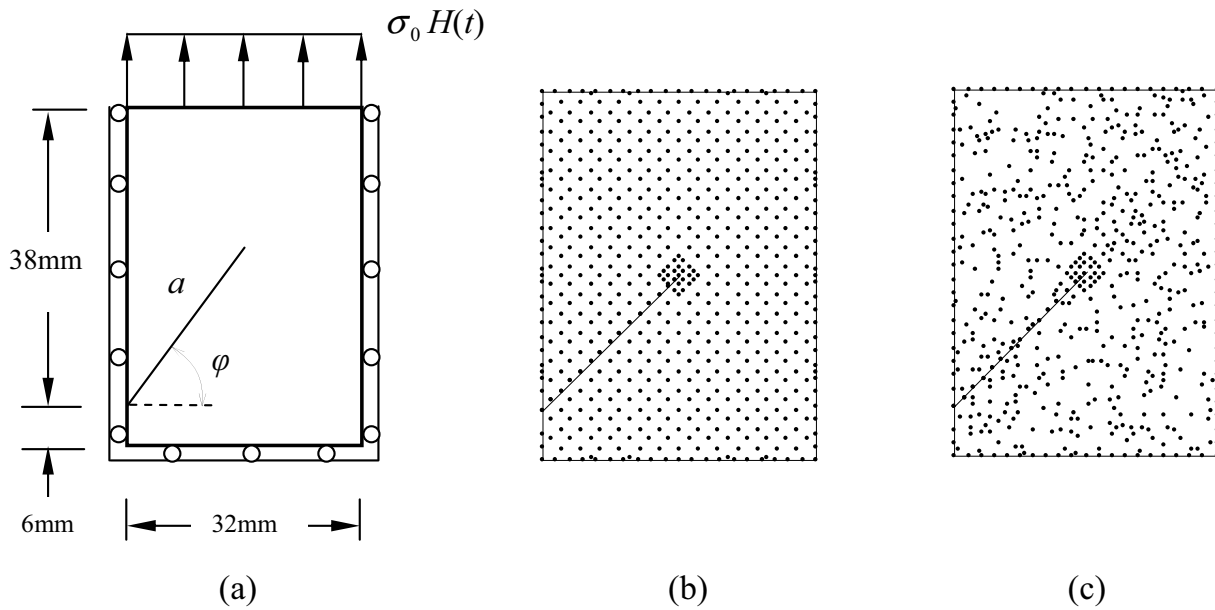


Figure 7: Geometry of a rectangular plate with an edge slant crack: (a) uniform tensile load at the ends; (b) regular distribution of nodes (637); (c) random distribution of nodes (600).

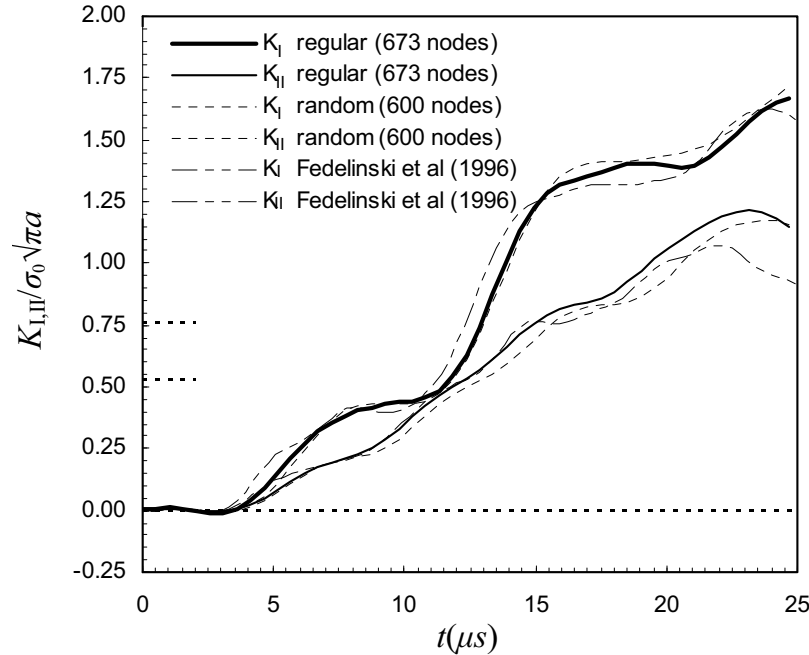
$E_1 \exp(\delta \sqrt{x_1^2 + x_2^2}/R)$, where $\delta = \ln(E_2/E_1)$. Table 2 shows the results of normalized stress intensity factor $K_I/\sigma_0\sqrt{\pi a}$ varying with the ratio of the Young's modulus E_2/E_1 for three cases. More accurate results are expected by using higher density for the node distribution.

5.4 A rectangular plate with an inclined edge crack under dynamic load

A rectangular plate with a crack slanted at an angle $\alpha = 45^\circ$ to the boundary with three edges simply supported shown in Fig.7(a) is instantaneously loaded by a uniform tensile stress $\sigma_0 H(t)$ (where H is a Heaviside function). The geometry of the cracked plate is shown in Fig.7(a) and

Table 2: SIFs $K_I/\sigma_0\sqrt{\pi a}$ for a central crack under tensile load

E_2/E_1	Case (a)		Case (b)		Case (c)	
	$N_{\text{total}} = 118$	$N_{\text{total}} = 370$	$N_{\text{total}} = 118$	$N_{\text{total}} = 370$	$N_{\text{total}} = 118$	$N_{\text{total}} = 370$
0.1	1.3792	1.5000	2.2529	2.2161	1.7446	1.8440
0.2	1.3115	1.4092	1.8651	1.8669	1.5761	1.6594
1.0	1.1778	1.2288	1.1778	1.2288	1.1778	1.2288
5.0	1.0883	1.1017	0.7515	0.8174	0.8058	0.8321
10.0	1.0631	1.0622	0.6302	0.6975	0.6642	0.6823

Figure 8: Dynamic stress intensity factors by different methods when $E_1 = E_0$.

the crack is of length $a = 22.63$ mm with angle $\phi=45^\circ$. The plate has the following material properties: Poisson ratio $\nu = 0.286$, shear modulus $\mu_0 = E_0/2(1 + \nu) = 29.4 \times 10^9$ Pa on the bottom of the plate and density $\rho = 2450$ kgm^{-3} (Poisson ratio and density are constants). The Young's modulus is graded along the crack exponentially as $E(x_2) = E_0 \exp(\delta x_2/h)$, where $h=44$ mm and $\delta = \ln(E_1/E_0)$. E_0 and E_1 denote the Young's modulus when $x_2 = 0$ and h respectively. The problem was solved using two types of distribution of the nodes, i.e. regular distribution with 637 nodes and random distribution with 600 nodes, as shown in Fig.7(b) and (c) respectively. Here, the method given by Durbin (1975) is employed. Demonstration of the Durbin's inverse method was made by Wen et al (1996) for elas-

todynamic fracture mechanics. For the Laplace transform, 26 transform parameters ($K=25$) are selected in this example. Figure 8 shows the normalized stress intensity factors $K_I(t)/K_0$ and $K_{II}(t)/K_0$ if $E_1/E_0 = 1$, where $K_0 = \sigma_0\sqrt{\pi a}$. The results given by Fedelinski et al (1996) using the dual boundary element method are plotted for comparison in this figure. The normalized stress intensity factors vs normalized time $c_1 t/b$, where $b=32$ mm and $c_1 = \sqrt{E(1-\nu)/\rho(1+\nu)(1-2\nu)}$ is the speed of longitudinal wave, are plotted in Figures 9 and 10 for three cases: $E_1/E_0 = 0.5, 1$ and 2. With a regular distribution of the nodes, the static stress intensity factors when $E_1/E_0 = 1$ are $K_I = 0.7575\sigma_0\sqrt{\pi a}$ and $K_{II} = 0.5273\sigma_0\sqrt{\pi a}$ respectively. These results are found to be within 5% of the accurate solutions by DBEM.

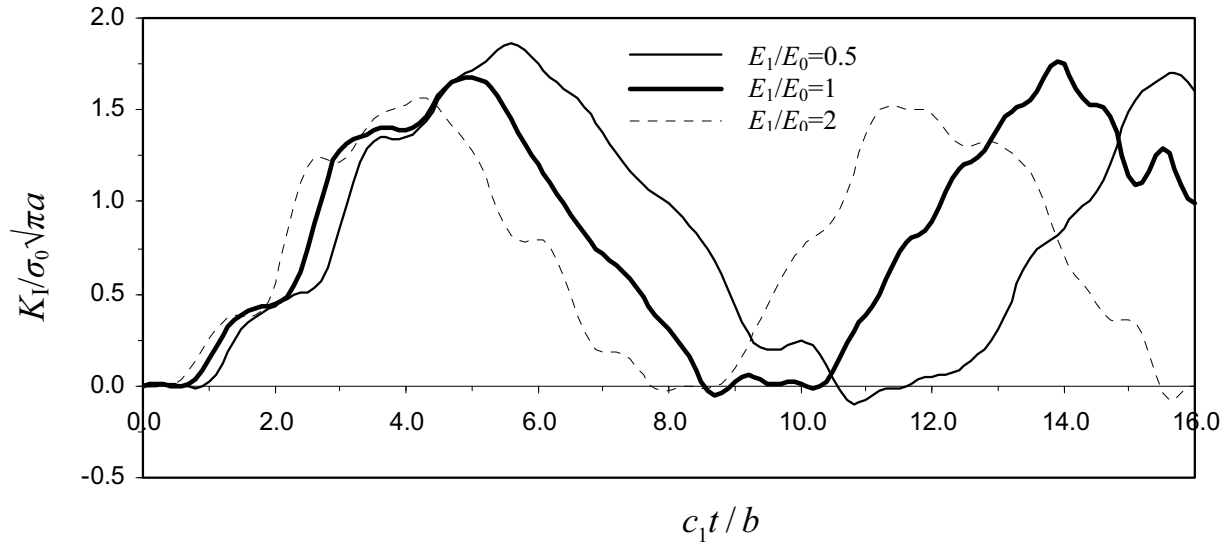


Figure 9: Time dependent normalized stress intensity factor $K_I/\sigma_0\sqrt{\pi a}$ for a rectangular plate with a slant edge crack under tensile Heaviside load.

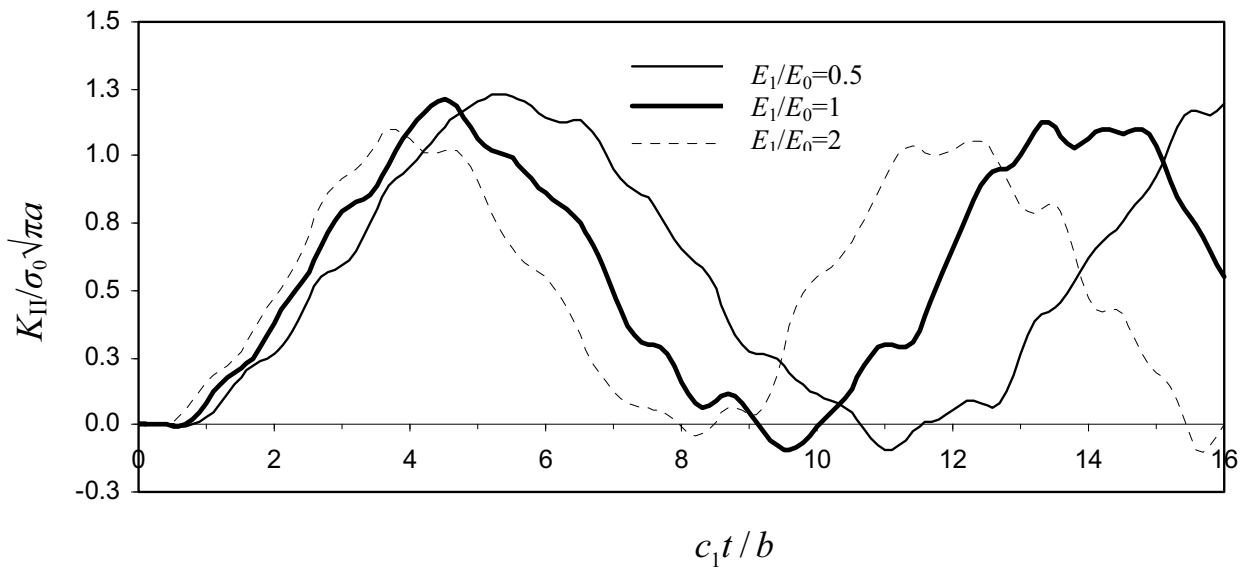


Figure 10: Time dependent normalized stress intensity factor $K_{II}/\sigma_0\sqrt{\pi a}$ for a rectangular plate with a slant edge crack under tensile Heaviside load.

6 Conclusions

By using enriched RBF interpolation in the local supported domain in this paper, the singular stresses ($1/\sqrt{r}$) at the crack tip can be captured. The external load and internal body forces can be treated as concentrated forces in the same way as FEM. The computational strategy of the accurate static and dynamic stress intensity factors of two-

dimensional mixed mode cracked structures with functionally graded materials have been demonstrated by several examples. We can conclude with the following observations: (1) The satisfied accurate SIFs can be obtained by enriched RBF for two dimensional static and dynamic problems; (2) Enriched RBF is more flexible and simpler to program than moving least square interpolation; (3) Similar to FEM, the stiffness matrix is

still symmetric and strip diagonal. Therefore, the combination of methods can be easily realised; (4) Proposed method can be easily developed to mixed mode problems and three-dimensional elasticity, plate bending and dynamic problems.

References

- Aliabadi, M.H.** (2002): *The Boundary Element Method, Vol 2: Applications in Solids and Structures*. Wiley: New York.
- Atluri, S.N.** (2004a): *The Meshless Method (MLPG) for Domain and BIE Discretizations*. Forsyth, GA, USA, Tech Science Press.
- Atluri, S.N.; Han, Z.D.; Rajendran, A.M.** (2004b): A New Implementation of the Meshless Finite Volume Method, Through the MLPG "Mixed" Approach, *CMES: Computer Modeling in Engineering and Sciences*, 6(6), 491-514.
- Atluri, S.N.; Han, Z.D.; Shen, S.** (2003): Meshless Local Petrov-Galerkin (MLPG) Approaches for Solving the Weakly-Singular Traction & Displacement Boundary Integral Equations, *CMES: Computer Modeling in Engineering and Sciences*, 4(5), 571-586.
- Atluri, S.N.; Liu, H.T.; Han, Z.D.** (2006): Meshless Local Petrov-Galerkin (MLPG) Mixed Collocation Method For Elasticity Problems, *CMES: Computer Modeling in Engineering and Sciences*, 14(30), 141-152.
- Atluri, S.N.; Shen, S.** (2002): The Meshless Local Petrov-Galerkin (MLPG) Method: A Simple & Less-costly Alternative to the Finite Element and Boundary Element Methods, *CMES: Computer Modeling in Engineering and Sciences*, 3 (1), 11-52.
- Atluri, S.N.; Zhu, T.** (1998a): A new meshless local Petrov-Galerkin (MLPG) approach to nonlinear problems in computational modelling and simulation, *Comput Model Simul Engng.*, 3, 187-196.
- Atluri, S.N.; Zhu, T.** (1998b): A new meshless local Petrov-Galerkin (MLPG) approach in computational mechanics, *Comput. Mech.*, 22, 117-127.
- Atluri, S.N.; Zhu, T.** (1999): The meshless local Petrov-Galerkin (MLPG) approach for solving problems in elasto-statics, *Comput. Mech.*, 25, 169-179.
- Atluri, S.N.; Liu, H.T.; Han, Z.D.** (2005): Meshless Local Petrov-Galerkin (MLPG) Mixed Finite Difference Method for Solid Mechanics, *CMES: Computer Modeling in Engineering and Sciences*, 15 (1), 1-16.
- Belytschko, T.; Lu, Y.Y.; Gu, L.** (1994): Element-free Galerkin method, *Int. J. Numerical Methods in Engineering*, 37, 229-256.
- Durbin, F.** (1975): Numerical inversion of Laplace transforms: an efficient improvement to Dubner and Abate's method. *The Computer J.*, 17, 371-376.
- Fedelinski, P.; Aliabadi, M.H.; Rooke, D.P.** (1996): The Laplace transform DBEM for mixed-mode dynamic crack analysis. *Computers & Structures*, 59(6), 1021-1031.
- Fleming, M.; Chu, Y.A.; Moran, B.; Belytschko, T.; Lu, Y.Y.; Gu, L.** (1997): Enriched element-free Galerkin methods for crack-tip fields, *Int. J. Numerical Methods in Engineering*, 40, 1483-1504.
- Han, Z.D.; Liu, H.T.; Rajendran, A.M.; Atluri, S.N.** (2006): The Applications of Meshless Local Petrov-Galerkin (MLPG) Approaches in High-Speed Impact, Penetration and Perforation Problems, *CMES: Computer Modeling in Engineering and Sciences*, 14(2), 119-128.
- Hardy, R.L.** (1971): Multiquadric equations of topography and other irregular surface, *J. Geophys. Res.*, 76, 1905-1915.
- Jarak, T.; Soric, J.; Hoster, J.** (2007): Analysis of shell deformation responses by the Meshless Local Petrov-Galerkin (MLPG) approach, *CMES: Computer Modeling in Engineering and Sciences*, 18 (3), 235-246.
- Kim, J.H.; Paulino, J.H.** (2002): Finite element evaluation of mixed mode stress intensity factors in functionally graded materials, *Int. J. Numerical Methods in Engineering*, 53, 1903-1935.
- Li, Q.; Shen, S.; Han, Z.D.; Atluri, S.N.** (2003): Application of Meshless Local Petrov-Galerkin (MLPG) to Problems with Singularities, and Ma-

terial Discontinuities, in 3-D Elasticity, *CMES: Computer Modeling in Engineering and Sciences*, 4(5), 517-586.

Li, S.; Atluri, S.N. (2008): Topology-optimization of structures based on the MLPG mixed collocation method, *CMES: Computer Modeling in Engineering and Sciences*, 26 (1), 61-74.

Liu, W.K.; Jun, S.; Zhang, Y. (1995): Reproducing kernel particle methods, *Int. J. Numerical Methods in Engineering*, 20, 1081-1106.

Ma, Q.W. (2008): A new meshless interpolation scheme for MLPG_R method, *CMES: Computer Modeling in Engineering and Sciences*, 23 (2), 75-89.

Nayroles, B.; Touzot, G.; Villon, P. (1992): Generalizing the finite element method: diffuse approximation and diffuse elements, *Computational Mechanics*, 10, 307-318.

Rao, B.N.; Rahman, S.A. (2001): Coupled meshless-finite element method for fracture analysis of cracks, *Int. J. Pressure Vessels and Piping*, 78, 647-657.

Sladek, J.; Sladek, V.; Zhang, Ch. (2004): Application of local integral equations to crack problems in FGMs, M.H. Aliabadi et al edited, *Advances in Fracture and Damage Mechanics IV*, EC Ltd, England, 155-160.

Sladek, J.; Sladek, V.; Zhang, Ch.; Solek, P. (2007a): Application of the MLPG to thermopiezoelectricity, *CMES: Computer Modeling in Engineering and Sciences*, 22 (3), 217-233.

Sladek, J.; Sladek, V.; Zhang, Ch.; Solek, P.; Starek, L. (2007b): Fracture analyses in continuously nonhomogeneous piezoelectric solids by the MLPG, *CMES: Computer Modeling in Engineering and Sciences*, 19 (3), 247-262.

Sladek, J.; Sladek, V.; Zhang, Ch.; Solek, P. (2007c): Application of the MLPG to Thermo-Piezoelectricity, *CMES: Computer Modeling in Engineering and Sciences*, 22(3), 217-234.

Sladek, J.; Sladek, V.; Krivacek, J.; Zhang, Ch. (2005a): Meshless local petrov-galerkin method for stress and crack analysis in 3-D axisymmetric FGM bodies, *CMES: Computer Modeling in*

Engineering and Sciences, 8(3), 259-270.

Sladek, V.; Sladek, J.; Tanaka, M.; Zhang, Ch. (2005b): Local integral equation method for potential problems in functionally graded anisotropic materials, *Engng Analy. with Boundary Elements*, 29, 829-843.

Wen, P.H.; Aliabadi, M.H. (2007): Applications of Meshless Method to Fracture Mechanics with Enriched Radial Base Functions, *Durability of Structures and Health Monitoring*, 3(2), 2007, 107-119.

Wen, P.H.; Aliabadi, M.H.; Rooke, D.P. (1996): The influence of elastic waves on dynamic stress intensity factors (three dimensional problem), *Archive of Applied Mechanics*, 66(6), 385-384.

